



Article

Plastic Deformation Characteristics and Calculation Models of Unbound Granular Materials under Repeated Load and Water Infiltration

Ning Li ^{1,2,3,*} , Xueyan Zhou ⁴, Dongxia Hu ⁵ and Jie Wang ^{1,*} 

¹ Key Laboratory of Transport Industry of Road Structure and Material, Research Institute of Highway, Ministry of Transport, Beijing 100088, China

² School of Civil Engineering, Xi'an University of Architecture and Technology, Xi'an 710055, China

³ Engineering Research Center of Green Construction & Smart Maintenance of Urban Infrastructure, Universities of Shaanxi Province, Xi'an 710055, China

⁴ School of Modern Post, Xi'an University of Posts & Telecommunications, Xi'an 710061, China; zhouxueyan@xupt.edu.cn

⁵ School of Road and Bridge Engineering, Xinjiang Vocational and Technical College of Communication, Urumchi 83140, China; hudongxia_xj@163.com

* Correspondence: lining_sn@xauat.edu.cn (N.L.); j.wang@rioh.cn (J.W.)

Abstract: Unbound granular materials (UGMs) have advantages in their water storage and drainage capabilities in permeable pavement, which is a benefit for urban sustainable development. The plastic strain of UGM is a crucial mechanical property that affects its design and construction. During its service life, repeated load only, repeated load after infiltration, and simultaneous action with load and infiltration are the three inevitable working conditions that will impact plastic strain, especially dynamic water infiltration. How these working conditions influence plastic strain needs to be focused on and solved. This study conducted laboratory tests to investigate plastic strain considering factors such as loading strength and repetitions, as well as infiltration number and duration. The results showed that the plastic strain and plastic strain rate exhibited similar variations during the repeated load only test and repeated load after infiltration test. The plastic strain changed significantly with different infiltration numbers but had relatively small variations in terms of the plastic strain rate. Longer infiltration duration led to greater plastic strain. With the simultaneous action, the plastic strain presented different variation to the other two conditions. The first and second infiltrations had a more obvious influence on the plastic strain when infiltration was applied. Calculation models were established to predict the effects of loading strength and repetitions as well as infiltration number and duration on plastic strains. For the repeated load only test, an error of 4.6% was observed. In terms of the infiltration number and duration, the errors were found to be 18.5% and 8.5%, respectively. The power function and Sigmoidal Logistic model were used to establish calculation models under the simultaneous action test with a maximum error of 11.5% ranging from 100 to 60,000 repetitions. The proposed calculation models can characterize plastic strain under the three working conditions very well, which can help in the design and construction of fully permeable pavement.

Keywords: unbound granular materials; plastic strain; repeated load; water infiltration; calculation model; simultaneous action



Citation: Li, N.; Zhou, X.; Hu, D.; Wang, J. Plastic Deformation Characteristics and Calculation Models of Unbound Granular Materials under Repeated Load and Water Infiltration. *Sustainability* **2023**, *15*, 14516. <https://doi.org/10.3390/su151914516>

Academic Editors: José Neves, Ana Cristina Freire and Vítor Antunes

Received: 12 September 2023

Revised: 29 September 2023

Accepted: 2 October 2023

Published: 6 October 2023



Copyright: © 2023 by the authors. Licensee MDPI, Basel, Switzerland. This article is an open access article distributed under the terms and conditions of the Creative Commons Attribution (CC BY) license (<https://creativecommons.org/licenses/by/4.0/>).

1. Introduction

Due to rapid urbanization and a reduction in water permeability, urban waterlogging has become a frequent occurrence. Additionally, the fully enclosed environment makes it hard for heat to exchange and release, resulting in an obvious heat island effect [1]. This has become an important factor restricting the sustainable development and ecological environment of cities. To alleviate this phenomenon, the concept of a “sponge city” has gained significant attention in recent years [2]. Permeable pavement has attracted much

attention for sustainable construction, which plays a crucial role in the construction of a “sponge city” as it can reduce urban waterlogging disasters, replenish groundwater resources and relieve the urban heat island effect [3,4]. During the construction of permeable pavement, unbound granular materials (UGMs) are one main layer that not only provide excellent support for superstructures but also possess strong storage and permeability capacities. Without mortar or cementitious material, UGM is a green and sustainable material that can be reused and constructed at room temperature. UGM provides an advantage for the application of fully permeable pavement and sustainable development. On the other hand, the performance of UGM directly influences the service level and lifespan of permeable pavement [5,6]. Water is the main consideration for the permeable pavement and UGM layer. During rainfall or sprinkling, water infiltrates into the UGM layer, leading to an increase in water content. Subsequently, excess water is drained away through the drainage or evaporation process, resulting in a reduction in water content over time [7]. Thus, the water content within the UGM layer undergoes dynamic changes during its service life. Besides water infiltration, vehicle loads are also an inevitable condition that permeable pavement will encounter. Under vehicle loads, the mechanical properties of the UGM are affected more or less. Among the various mechanical properties of UGM, plastic strain is one of the most important indicators that is significantly affected by vehicle loads. The vehicle loads frequently exert force on permeable pavement, which is the main factor causing plastic strain. More importantly, previous studies have proved that water content has a significant impact on the deformation behavior of UGM [8–10]. With this condition, plastic strain is influenced by both vehicle load and water infiltration. The characteristics of plastic strain have become a valuable point for developing reasonable strategies for the construction of permeable pavement. However, limited research is available to investigate the deformation properties of UGM under infiltration and repeated load conditions, especially the dynamic moisture content.

Due to the stress-dependent characteristics of UGM, most studies primarily focused on the influence of repeated load using various testing methods. Using repeated load triaxial tests (RLTT), plastic strain was analyzed by Tseng and Lytton, Lekarp, and Werkmeister et al., who provided calculation models of plastic strain considering the repeated load only [11–13]. Hornyk and Erlingsson et al. investigated the influence of stress levels and paths on plastic strain via multistage triaxial tests [14,15]. To simplify the triaxial test, Araya developed the repeated California bearing ratio (CBR) test to characterize the properties of UGM, estimating both the plastic strain and resilient modulus [16]. In addition, Li et al. analyzed the plastic strain of UGM using a precision unbound material analyzer (PUMA) with up to 100,000 loading repetitions and established a plastic strain model considering the loading condition and material composition [17,18]. Besides the loading, the gradation of composition, compactness and moisture content were also examined in previous studies [19–23]. The effects of grading, composition and compactness on the permanent strain of UGM were also studied using RLTT by Gu et al. [19]. Based on the theory of maximum density curve and packing theory, coarse aggregate was regarded as the skeleton material and fine aggregate acted as the filler to ensure that the UGM had a maximum density with a stable skeleton structure [20,21]. Considering the influence of water on the UGM's behavior, permeability evaluation is commonly employed. Li et al. tested and evaluated the permeability of UGM using self-designed equipment [22]. Kazemi et al. found that base coarse aggregates could improve the capacity of water infiltration [23]. The deformation of five open-graded base materials was compared by Ma et al., who found that UGM can provide good mechanical properties for permeable pavement [6]. Sangsefidi et al. investigated the effect of wetting and drying cycles on the performance of two aggregates via the California bearing ratio (CBR) and repeated load triaxial tests [9]. Although water content was involved in RLTT, repeated CBR or PUMA tests, it was usually designed at a specific value. However, the dynamically adjusted water content not only affected the friction between the gravel particles but also had a water-scouring effect on the permeable pavement. The coupling effect of dynamic water

led to differences between specific and static water on the plastic strain of the UGM. Under this condition, repeated load only was insufficient for the plastic strain investigation of UGM in permeable pavement. Thus, more attention needs to be paid to the effects of water infiltration.

To investigate the influence of water infiltration and vehicle loads on the properties of UGM, Xiao et al. introduced a new gradation design concept intended for controlling stability and field drainability [24,25]. However, plastic deformation was not emphasized and analyzed with long loading repetitions, nor were the working conditions considered beyond their limited scope. When water infiltrates into permeable pavement, several working conditions exist. Among them, typically, vehicle loads are exerted subsequently to water infiltration, and the vehicle loads act simultaneously with the water infiltrates. Then, there are three working conditions for UGM in permeable pavement: repeated load only, repeated load after infiltration, and simultaneous action with load and infiltration, respectively. Taking the working conditions into account, Li et al. conducted experimental tests to investigate the effect on the water-retention, particle migration and bearing capacity of UGM considering the influence of infiltration [26]. However, plastic strain was not fully analyzed and compared. It is necessary to find out the deformation characteristics of UGM under repeated load and water infiltration conditions so as to provide valuable guidance for the design and construction of permeable pavement.

In this study, the objective was to investigate the plastic deformation of UGM in permeable pavement under different load and water infiltration conditions. Three working conditions were used, which were repeated load only, repeated load after infiltration, and simultaneous action with load and infiltration. During the tests, loading strength, loading repetitions, infiltration number and infiltration duration were taken as the factors. Considering the main influence factor of this study, the used gradation of UGM was the median with 96% compactness at optimum moisture content. The improved PUMA test method was used for the investigation, which we referenced from a previous study in the literature [26]. In this study, the plastic strain and plastic strain rate were the main analysis indicators, the relationship between plastic strain and plastic strain rate, and the elasto-plastic total strains, were also analyzed. To quantitatively evaluate the plastic strain of the UGM, several calculation models were established under the three working conditions. With these models, the plastic strain was calculated considering the load and infiltration factor. This can benefit the understanding of UGM and their application in fully permeable pavement. More importantly, the UGM layer has the advantage of enabling sponge city construction and alleviates the urban heat island effect, which has great significance for the sustainable development of cities.

2. Materials and Methods

2.1. Test Materials

In this study, the used aggregate was crushed limestone, produced in Tongchuan. According to the test methods in JTG E42-2005, the properties of coarse and fine aggregate met with the requirements in JTG/TF20-2015 [27,28]. The designed composition of the UGM was median gradation according to the specifications in JTG/TF20-2015 [28], as shown in Figure 1. The coefficient of curvature C_c and non-uniformity C_u were 2.69 and 19.34, respectively. The specification stipulates that the soil has a well gradation when C_u is greater than 5 and C_c is between 1 and 3. This indicated that the UGM had a well gradation. Using the compaction test method in JTG E40-2007 [29], the maximum dry density of the designed gradation was 2.386 g/cm³ and the optimal moisture content was 5.3%.

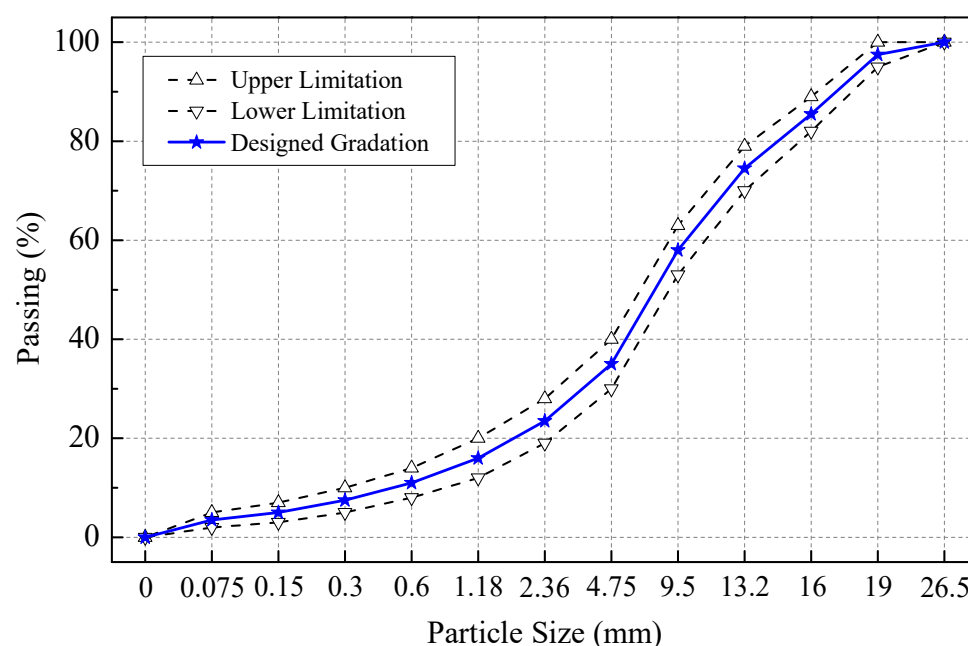


Figure 1. Gradation curve of the designed gradation.

2.2. Test Method

The conducted tests utilized the improved PUMA method that has been comprehensively described in the literature [26,30,31]. Three category of tests were carried out: a repeated load only test, repeated load test after infiltration, and simultaneous action with load and infiltration test, respectively. During the tests, the loading strengths were 80 kPa, 160 kPa, 240 kPa and 320 kPa, at a frequency of 5 Hz, and with a total of 20,000 repetitions. The infiltration was conducted with varying numbers (0, 1, 2, 3, 4 and 5) and durations (10 min, 60 min and 240 min). Each group had three parallel tests.

As for the simultaneous action with load and infiltration test, the action time for repeated load was 66.7 min when the loading repetitions were set at 20,000 and the frequency was at 5 Hz. It was observed that the loading action time was considerably different from the 240 min infiltration duration. The duration for infiltration and repeated loading cannot be enacted simultaneously all the time. Therefore, the infiltration duration was adjusted to 10 min (3000 loading repetitions), 35 min (10,000 loading repetitions) and 60 min (18,000 loading repetitions) for the simultaneous action test. In addition, the simultaneous action tests were performed with three cycles. The experimental plan of the three categories is presented in Table 1.

According to the features of the PUMA equipment, the plastic strain, elastic strain, confining stress, stiffness modulus and Poisson's ratio can be obtained [26,30,31]. In this study, the purpose was to establish a plastic strain model under different working conditions. Then, the plastic strain was the primary analysis indicator. To effectively characterize the variation in plastic strain with loading repetitions, the plastic strain rate was also employed. It should be noted that the plastic strain rate was the increment in plastic strain between two adjacent loading repetitions, which is different from the definition in elasto-plastic theory. Loading strength and repetitions, and the infiltration number and duration, were taken as the influence factors.

Table 1. Experimental plan of the repeated load and infiltration.

Working Conditions	Serial Number	Loading			Infiltration		Materials		
		Loading Strength	Loading Frequency	Loading Repetitions	Number	Duration	Gradation Type	Compactness	Moisture Content
Repeated load only	1	80 kPa	5 Hz	20,000	0	0	Median	96%	5.3%
	2	160 kPa	5 Hz	20,000	0	0	Median	96%	5.3%
	3	240 kPa	5 Hz	20,000	0	0	Median	96%	5.3%
	4	320 kPa	5 Hz	20,000	0	0	Median	96%	5.3%
Repeated load after infiltration	5	160 kPa	5 Hz	20,000	1	60 min	Median	96%	5.3%
	6	160 kPa	5 Hz	20,000	2	60 min	Median	96%	5.3%
	7	160 kPa	5 Hz	20,000	3	60 min	Median	96%	5.3%
	8	160 kPa	5 Hz	20,000	4	60 min	Median	96%	5.3%
	9	160 kPa	5 Hz	20,000	5	60 min	Median	96%	5.3%
	10	160 kPa	5 Hz	20,000	1	10 min	Median	96%	5.3%
	11	160 kPa	5 Hz	20,000	1	240 min	Median	96%	5.3%
Simultaneous action with load and infiltration	12	160 kPa	5 Hz	20,000	1	10 min	Median	96%	5.3%
	13	160 kPa	5 Hz	20,000	1	35 min	Median	96%	5.3%
	14	160 kPa	5 Hz	20,000	1	60 min	Median	96%	5.3%
	15	160 kPa	5 Hz	40,000	2	10 min	Median	96%	5.3%
	16	160 kPa	5 Hz	40,000	2	35 min	Median	96%	5.3%
	17	160 kPa	5 Hz	40,000	2	60 min	Median	96%	5.3%
	18	160 kPa	5 Hz	60,000	3	10 min	Median	96%	5.3%
	19	160 kPa	5 Hz	60,000	3	35 min	Median	96%	5.3%
	20	160 kPa	5 Hz	60,000	3	60 min	Median	96%	5.3%

3. Plastic Strain and Plastic Strain Rate Analyses

3.1. Plastic Strain

Based on the experimental plan in Table 1, the plastic strain of the UGM was obtained under the three working conditions, as shown in Figure 2. Under the repeated load only and repeated load after infiltration tests, the plastic strain presented the same features. In the initial stage of repeated load, the plastic strain rapidly increased and accumulated. However, the plastic strain gradually became stable with the increase in loading repetitions. This trend was consistent with previous results, where the plastic strain increased rapidly in the early stage, and became stable after several thousand loading repetitions from the laboratory tests and field monitoring, which was pointed out by Wolff, Visser, and Dawson et al. [32,33]. This is related to the characteristics of shakedown and typical elasto-plastic properties, which is an inherent attribute for granular materials. Under lower loading strength, UGM can bear the load via the contact of particles, and the particles tend to migrate so as to form stronger contact when the loading strength becomes greater. Therefore, greater plastic strain is produced under greater loading strength.

From the perspective of loading strength, the plastic strain was proportional to the loading strength. Greater loading strength contributed to greater plastic strain due to the stress-dependent characteristic of the UGM. Compared with the repeated load only test, the plastic strain increased significantly after infiltration, as shown in Figure 2b. The plastic strain continued to increase with the increase in infiltration number. However, the increment of plastic strain was significantly decreased and tended to be in a stable state. To clearly display the plastic strain under different factors, Table 2 shows the plastic strain experienced at 20,000 loading repetitions. With 2 to 5 times the infiltration, the differences in plastic strain were not so significant. The maximum difference in plastic strain was only 0.5094×10^{-3} after 20,000 repetitions. This indicated that the effect of infiltration number on plastic strain was limited, and the significant influence occurred mainly in the first and second infiltrations.

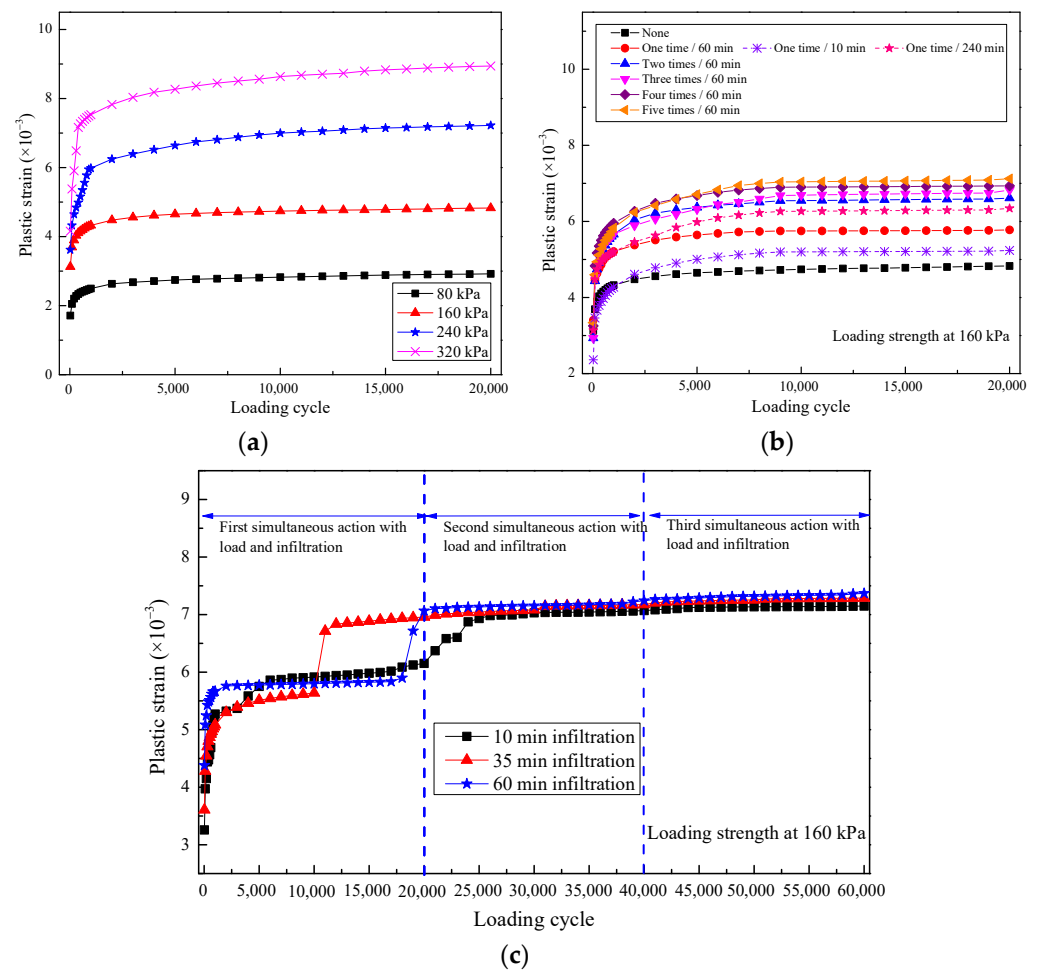


Figure 2. Plastic strain of UGM under three working conditions: (a) repeated load only; (b) repeated load after infiltration; (c) simultaneous action with load and infiltration.

Table 2. Plastic strain ($\times 10^{-3}$) with 20,000 loading repetitions.

Repeated Load Only		Repeated Load after Infiltration		Simultaneous Action with Load and Infiltration	
80 kPa	2.922	One time	5.777	10 min (20,000)	6.151
160 kPa	4.828	Two times	6.614	35 min (20,000)	6.957
240 kPa	7.223	Three times	6.825	60 min (20,000)	7.066
320 kPa	8.942	Four times	6.934	10 min (40,000)	7.069
--	--	Five times	7.123	35 min (40,000)	7.175
--	--	10 min	5.238	60 min (40,000)	7.241
--	--	240 min	6.344	10 min (60,000)	7.148
--	--	--	--	35 min (60,000)	7.287
--	--	--	--	60 min (60,000)	7.369

With the one-time repeated load after infiltration test, the plastic strain increased with the increase in infiltration duration. The longer duration led to greater plastic strain under the repeated load. Although there was a positive correlation, the plastic strain was not in proportion to infiltration duration. When the duration increased from 10 min to 60 min, the difference in plastic strain was 0.5673×10^{-3} . The value was only 0.5024×10^{-3} when the duration increased from 60 min to 240 min. This showed that the influence of infiltration duration on the plastic strain decreased when it exceeded a certain value. The

greater influence of infiltration on the plastic strain mainly occurred within 60 min and two infiltrations. This is because water infiltration affects the friction and voids among the particles. When water enters into the UGM, the friction decreases, leading to the easier migration of particles. However, the effect of friction reduction was limited. Then, the differences in plastic strain were not so significant with three or more infiltration numbers and 60 min or longer infiltration durations.

When the repeated load and infiltration acted simultaneously, the plastic strain was different from the previous two working conditions, as shown in Figure 2c. An obvious increase occurred during the subsequent loading process when the infiltration ended in the first simultaneous action. It is worth noting that the variation in plastic strain with 10 min infiltration was different from that under the other conditions. With 10 min simultaneous action, the plastic strain was greater than the other conditions during 5000 to 20,000 repetitions. This phenomenon was unusual compared to the previous results. It was speculated that the action of dynamic water-scouring was enhanced with a short period once the infiltration stopped. Then, there would be a greater increment during the following several hundred repetitions. Based on this speculation, we can also explain the variation with 35 min and 60 min infiltration. Then, the plastic strain with 10 min infiltration had a greater value due to the occurrence of a transient water-scouring enhancement. After the first simulation action, the increments of plastic strain were 0.2161×10^{-3} , 1.0735×10^{-3} and 0.8169×10^{-3} , corresponding to 10 min, 35 min and 60 min infiltration, respectively. The variation range was up to 19%. This indicated that the simultaneous action had a significant influence on the plastic strain, and the most significant effect was obtained with 35 min infiltration. In the initial stage of the second simultaneous action (about 20,000~25,000 repetitions), the plastic strain increased significantly with 10 min infiltration. By contrast, the plastic strain did not fluctuate significantly during the second simultaneous action with 35 min and 60 min infiltration. During the third simultaneous action, the plastic strain increased a small amount with the three durations, which had increments of 0.0791×10^{-3} , 0.1121×10^{-3} and 0.1279×10^{-3} for 10 min, 35 min and 60 min, respectively. The maximum increase magnitude was only 1.77%. In addition, the plastic strain presented a linear variation trend with the loading repetitions. This showed that the infiltration action had a small effect on the plastic strain under the third simultaneous action. As seen from the value of plastic strain at the end of the three simultaneous actions, the plastic strain with 10 min infiltration was significantly smaller than that with 35 min and 60 min infiltration. The plastic strain was close with 35 min and 60 min infiltration, where the difference was only 0.1091×10^{-3} . After two simultaneous actions, the plastic strain values were approximately the same under the different conditions.

The following reasons can be attributed to the above phenomena. First, the contact relationship of gravel particles is greatly affected by the water flow when the first infiltration action occurs, while this influence becomes slight during subsequent water flow. Then, the difference is small after the first simultaneous action, which is related to the reduced influence of the infiltration action on the UGM, as mentioned before [26]. Second, the migration of gravel particles is accelerated due to the action of water, contributing to the formation of a stable structure. The UGM has a typical characteristic of shakedown, in which the plastic strain reaches a stable state after a certain number of repetitions [13,34]. Therefore, the plastic strain varies greatly under the first and second simultaneous actions, while it changes little under the third simultaneous action. Third, the loss of some fine aggregate during the infiltration action also leads to the migration of gravel particles [26]. Fourth, as the PUMA test is a full cross-section loading mode, the water film forms on the sample surface, which may lead to a water-buffering effect. The difficulty of water entering the sample increased significantly during the second and third simultaneous action compared to the first action. Then, the plastic strain changed little during the later simultaneous actions.

3.2. Plastic Strain Rate

The variation in plastic strain rate presented considerable differences with the plastic strain under the three working conditions, as shown in Figure 3. Under different working conditions, the plastic strain rate had a similar variation tendency with loading repetitions. The plastic strain rate rapidly declined at the initial stage of repeated load, and then, tended to be stable. After 20,000 repetitions, the plastic strain rate reached a level of 10^{-7} – 10^{-9} /cycle. At this time, the plastic strain basically remained stable. Actually, the plastic strain had little increase with the repetitions of the repeated load. This was consistent with the characteristics of the shakedown behavior for granular materials. Under the same loading strength level, the plastic strain was limited so that the plastic strain rate became smaller and smaller along with the loading repetitions. As for the repeated load after infiltration test, the plastic strain rate was about ten times smaller (mainly 10^{-8} – 10^{-9} /cycle) than that under the repeated load only test, and the variation was relatively more stable. However, the plastic strain rate under the simultaneous action test had great fluctuation that ranged from 10^{-6} /cycle to 10^{-9} /cycle. The plastic strain rate decreased step by step when three simultaneous actions were carried out. Great variation appeared at the end of the previous infiltration and the beginning of the next infiltration. This showed that infiltration accelerated the process of particle stabilization, leading to great fluctuation of the plastic strain rate when infiltration was carried out. It was noted that fluctuation hardly affected the stabilization tendency of the plastic strain rate, and the influence of infiltration was small when the number of loading repetitions was greater than 10,000.

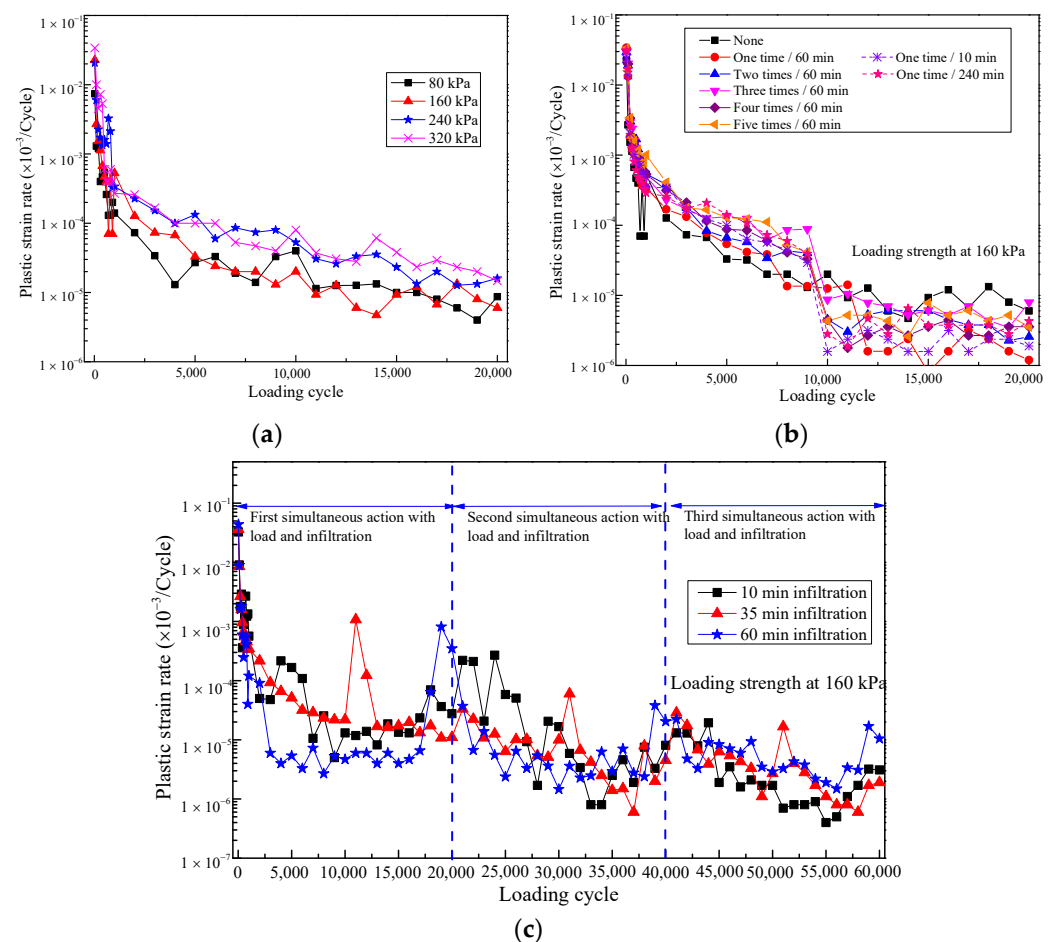


Figure 3. Plastic strain rate of the UGM under three working conditions: (a) repeated load only; (b) repeated load after infiltration; (c) simultaneous action with load and infiltration.

3.3. Relationship between Plastic Strain and Plastic Strain Rate

Based on the characteristics of plastic strain and plastic strain rate in Figures 2 and 3, the relationship between them is shown in Figure 4 with linear and logarithmic vertical ordinates. In the linear coordinate system, a downward convex parabolic relationship existed under the three working conditions. When the plastic strain was small, the plastic strain rate changed fast, and it approached zero when the plastic strain increased to a certain extent. This was consistent with previous conclusions that plastic strain reached a stable value after a certain number of loading repetitions [13,34]. As shown in the subgraph in the upper right corner, the variation tendency was different under the three tests in the logarithmic vertical ordinate system. The variations were similar under the repeated load only and repeated load after infiltration tests. However, they fluctuated greatly under the simultaneous action test. There was an obvious turning point that corresponded to the beginning time of the simultaneous actions. According to the characteristics of the PUMA test, the stress state changed sharply when the loads started to be exerted. Then, there was a great increment in the plastic strain at the initial stage of load action. Therefore, the plastic strain rate at the beginning stage of the second and third simultaneous actions had a significant increase and a turning point. These phenomena indicated that the plastic strain was also affected by the intermittent infiltration. It was necessary to consider the number of infiltrations.

In the logarithmic vertical ordinate system, Figure 4 shows that the plastic strain and plastic strain rate had an approximately linear relationship, which can be fitted using the linear fitting model in Equation (1).

$$\ln(\dot{\varepsilon}_p) = a\varepsilon_p + b \quad (1)$$

where ε_p is the plastic strain, $\dot{\varepsilon}_p$ is the plastic strain rate, and a and b are the model parameters. With this fitting model, the correlation coefficients were acquired under various factors. The *adjusted-R²* is shown in Table 3. The repeated load only test had the greatest correlation coefficient, which ranged from 0.915 to 0.945. As for the repeated load after infiltration test, the linear correlation coefficient was 0.786 to 0.851, while it was only 0.356 to 0.737 for the simultaneous action test. This showed that the relationship between plastic strain and plastic strain rate was different under the three working conditions. Among them, the simultaneous action test had a poor linear correlation related to the enhanced effect of loading and infiltration, especially the period during the beginning and end of infiltration. Under the repeated load only test, the plastic strain was only affected by the loading without other interference. The variation in plastic strain was smooth and stable so that the *adjusted-R²* had the greatest value. When the UGM suffered from water infiltration, the moisture content and migration tendency of the particles increased.

Table 3. *Adjusted-R²* of fitting results of plastic strain and plastic strain rate.

Repeated Load Only		Repeated Load after Infiltration		Simultaneous Action with Load and Infiltration	
Factor	<i>Adj-R²</i>	Factor	<i>Adj-R²</i>	Factor	<i>Adj-R²</i>
80 kPa	0.948	One time	0.786	10 min	0.737
160 kPa	0.915	Two times	0.809	35 min	0.753
240 kPa	0.924	Three times	0.845	60 min	0.356
320 kPa	0.917	Four times	0.851	--	--
--	--	Five times	0.826	--	--
--	--	10 min	0.808	--	--
--	--	240 min	0.827	--	--

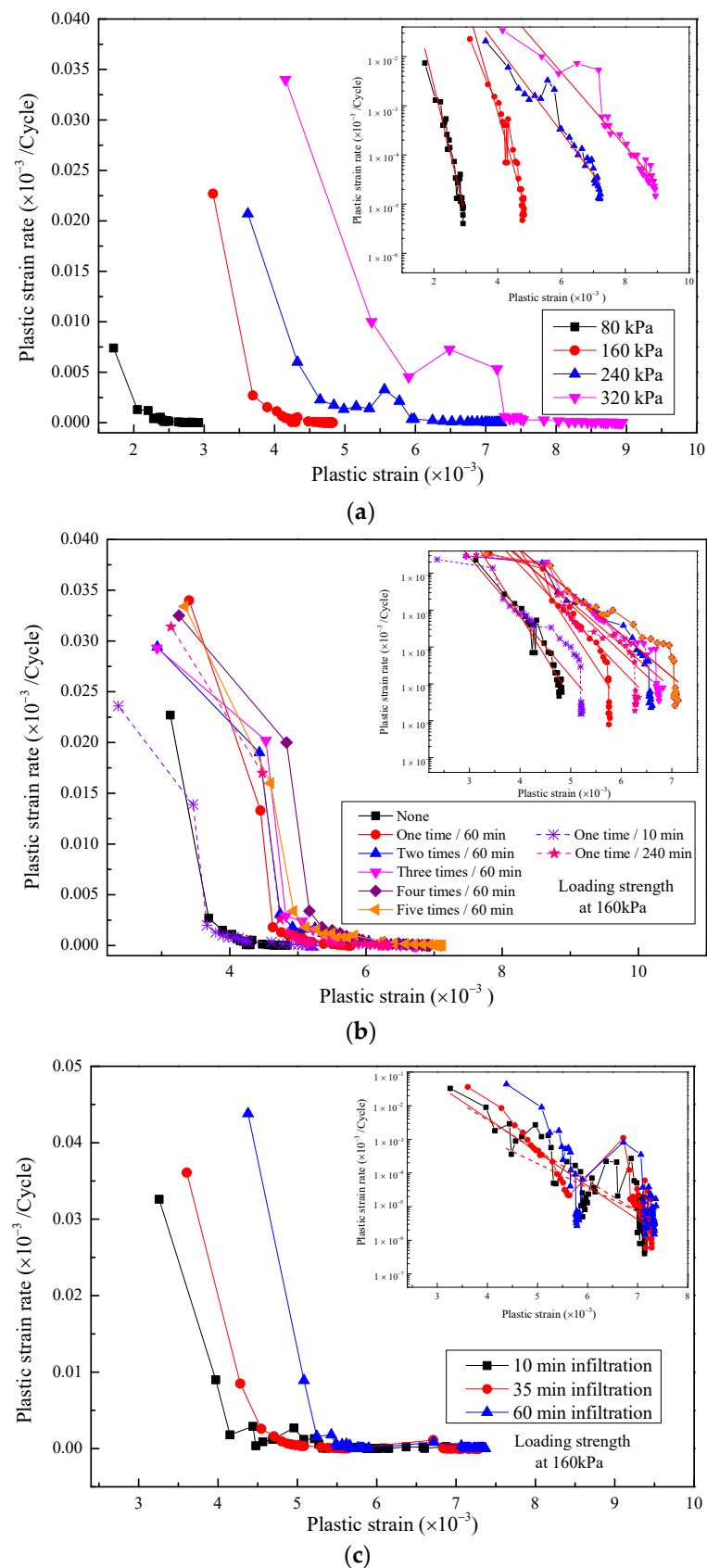


Figure 4. Relationship between plastic strain and plastic strain rate of the UGM under three working conditions: (a) repeated load only; (b) repeated load after infiltration; (c) simultaneous action with load and infiltration.

3.4. Elasto-Plastic Total Strain

With the three working conditions, the elasto-plastic total strain is shown in Figure 5. The plastic strain accounted for 91~96% of the total strain under the different conditions, while the elastic strain accounted for less than 9%. By contrast, the variation in total strain was greatly consistent with plastic strain. The total strain increased with the increase in loading strength, infiltration duration and number. Compared with repeated load after infiltration test, the plastic strain and total strain changed greatly under the simultaneous action test, while the elastic strain varied little. Under the simultaneous action test, the maximum difference in the total strain was only 0.3185×10^{-3} , which only accounted for 4.2% of the average total strain (7.5198×10^{-3}). This indicated that the total strain had little difference under the three simultaneous actions. However, compared with the repeated load only test, the total strain increased by 2.24×10^{-3} (accounting for 42.4%) under the simultaneous action. The value was 1.282×10^{-3} (accounting for 20.6%) compared with the repeated load after infiltration test. These differences showed that the increments were mainly caused by water infiltration. With water infiltration, the particles had a great tendency to migrate once the load was exerted, resulting in a larger total strain. The simultaneous action had an especially significant effect. There was not only load action, but also a dynamic water-scouring effect, leading to greater strain. Whether the repeated load followed or simultaneously acted with infiltration, the infiltration action had an important effect on the total strain of the UGM. Therefore, careful consideration should be given to the infiltration condition during the design and construction of UGM layers in permeable pavement.

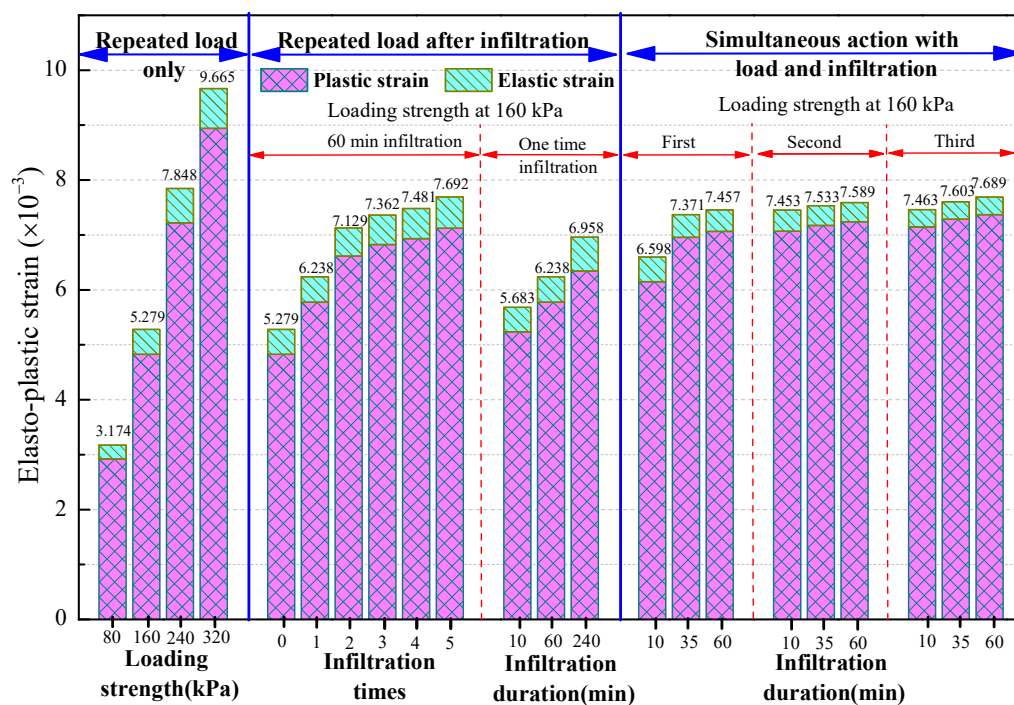


Figure 5. Elasto-plastic strain of the granular material under three working conditions.

4. Plastic Strain Calculation Model under Three Working Conditions

Under the three working conditions, the plastic strain was obtained and compared. To establish a quantitative description, fitting regression was conducted to establish a calculation model for the plastic strain of the UGM. The mentioned factors were involved in the calculation models.

4.1. Repeated Load Only

Previous studies have proposed different models to describe the variation in plastic strain with loading repetitions [18,33]. These models are all based on the power function model as follows:

$$\varepsilon_p = aN^b \quad (2)$$

where ε_p is the plastic strain, N is the number of loading repetitions, and a and b are the model parameters. This model can effectively characterize the plastic strain in the significant nonlinear stage of the UGM under repeated loads. Using the model in Equation (2), the calculation model parameters of plastic strain at four loading strength are shown in Table 4.

Table 4. Parameter fitting results of plastic strain model at four loading strengths.

Parameters	Loading Strength			
	80 kPa	160 kPa	240 kPa	320 kPa
a	1.5327	2.8198	2.8534	3.8349
b	0.0671	0.0521	0.0972	0.0894
$Adj-R^2$	0.964	0.9395	0.9695	0.8908

As seen in Table 4, the goodness of fit of the plastic strain model was greater than 0.9 at different loading strengths. This showed that the model can effectively characterize the plastic strain under this condition. Although the model in Equation (2) had better performance, it was only appropriate for a certain loading strength. Considering the loading strength, parameters a and b were analyzed. The relationship was fitted between parameters a and b to loading strength using a power model and a linear model, respectively. The fitting results are shown in Table 5.

Table 5. Fitting results of parameters a and b to loading strength.

Parameters	a	b	$Adj-R^2$
Expressions	$a = 0.1105 \times \sigma_d^{0.6138}$	$b = 0.0001 \times \sigma_d + 0.0485$	0.9019/0.4905

With the expressions of a and b in Table 5, the plastic strain model under the repeated load only test can be rewritten using Equation (3) as follows:

$$\varepsilon_p = 0.1105 \times \sigma_d^{0.6138} \times N^{(0.0001 \times \sigma_d + 0.0485)} \quad (3)$$

where ε_p is the plastic strain (10^{-3}), σ_d is the loading strength (kPa), and N is the number of loading repetitions. Using Equation (3), the plastic strain can be calculated as shown in Figure 6. In addition, the measurements are displayed to make comparisons. This shows that the calculated plastic strain at 80 kPa had relatively good coordination with the measurements, while the calculation at other loading strengths greatly differed from the measurements. The maximum difference was up to 4.3657×10^{-3} . This showed that the model in Equation (3) cannot effectively calculate the plastic strain at different loading strengths. This was because the parameters a and b had great sensitivity to the model, which had four parameters. Any changes would have a great impact on the results.

At different loading strengths, the plastic strain presented great similarities. The plastic strain at other loading strengths was linearly fitted with that at 80 kPa, as shown in Figure 7. The correlations were greater than 0.97, indicating that the variation trend of plastic strain was highly similar at different loading strengths. The plastic strain at different loading strengths had a good linear correlation with the plastic strain at 80 kPa. Therefore, the plastic strain at 80 kPa was taken as the baseline for linear fitting using the model $\varepsilon_p = k \times aN^b + c$. The fitting parameters k and c are shown in Table 6.

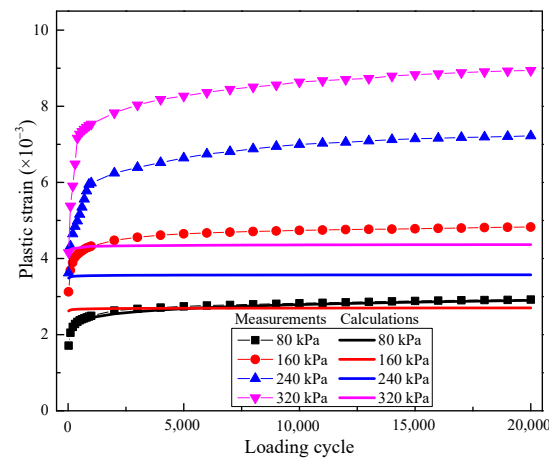


Figure 6. Plastic strain comparison between measurements and calculations.

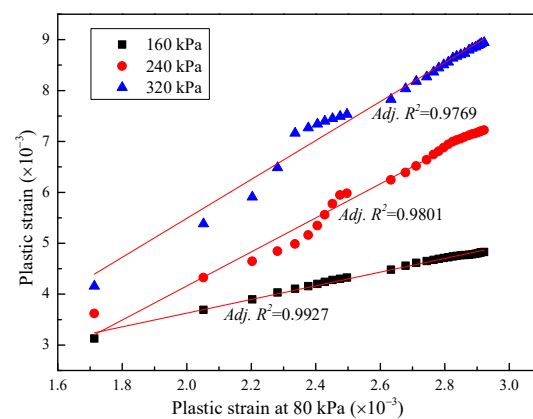


Figure 7. Relationship of plastic strain at 80 kPa and other strengths.

Table 6. Fitting results of parameters k and c to loading strength.

Parameters	k	c	Adj- R^2
Expressions	$k = 0.0131 \times \sigma_d - 0.2404$	$c = -0.0124 \times \sigma_d + 1.5479$	0.9149/0.5869

With the expressions of k and c in Table 6, the plastic strain model was obtained at different loading strengths for the repeated load only test, as shown in Equation (4).

$$\varepsilon_p = (0.0131 \times \sigma_d - 0.2404) \times N^{0.0671} + (-0.0124 \times \sigma_d + 1.5479) \quad (4)$$

where ε_p is the plastic strain (10^{-3}), σ_d is the loading strength (kPa), and N is the number of loading repetitions. Using Equation (4), the plastic strain was calculated at various loading strengths and repetitions, as displayed in Figure 8. In addition, the calculations were compared with the measurements. The results showed that the calculations and measurements kept great compatibility at different loading strengths and repetitions. Among them, the maximum difference was 0.4111×10^{-3} , accounting for only 4.6% of the measurements. Moreover, compared with the calculations obtained using Equation (4), the differences from Equation (5) and measurements were reduced by 10 times. This indicated that the model in Equation (5) had greatly accuracy for the plastic strain calculation at different loading strengths under the repeated load only test.

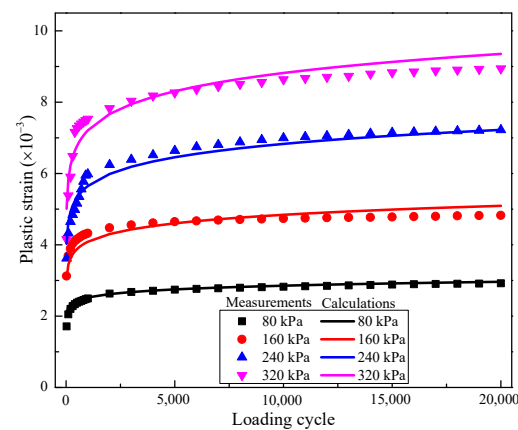


Figure 8. Plastic strain measurements and calculations at four loading strengths.

4.2. Repeated Load after Infiltration

As for the plastic strain in the repeated load after infiltration test in Figure 2b, it presented a similar variation tendency at different infiltration numbers and durations. Therefore, the plastic strain calculation model can be established using the method in the repeated load only test. Three steps can be drawn for the calculation model as follows.

- Step 1: Establish the initial plastic strain model (using Equation (3)) for the condition that no infiltration and only the repeated load was applied.
- Step 2: Establish the correlation model between the plastic strain at other infiltration numbers and durations with the plastic strain at no infiltration.
- Step 3: Establish the final calculation model of plastic strain at different infiltration numbers and durations.

Taking the plastic strain at non-160 kPa (test serial number 2) and one-time 60 min infiltration (test serial number 5) as the baseline, the relationships between the baseline and plastic strain at different infiltration numbers and durations are shown in Figure 9. With the correlation analyses in step 2, the parameters k and c of the calculation model ($\epsilon_p = k \times aN^b + c$) are shown in Table 7. The linear correlation coefficients between the infiltration factors and baseline were as great as 0.99 or more. This showed that the plastic strain had very high similarities under different infiltration conditions.

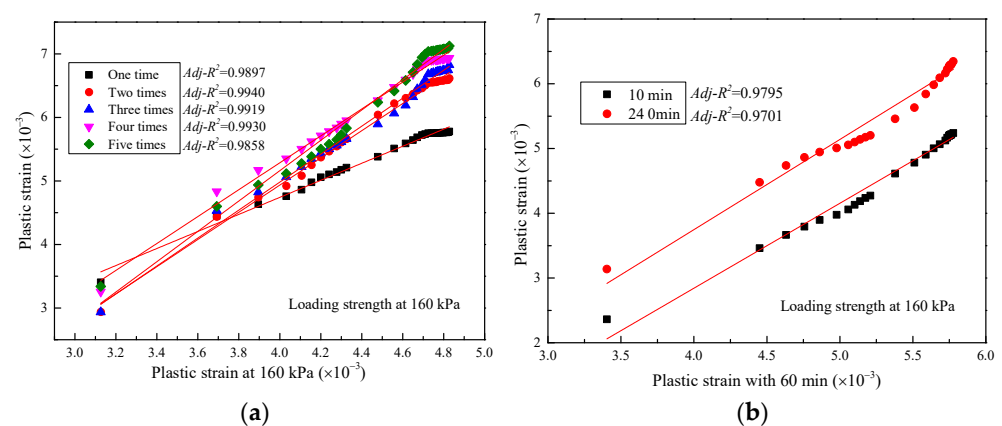


Figure 9. Relationship of plastic strain at 160 kPa and 60 min with other infiltration conditions: (a) infiltration numbers; (b) infiltration durations.

Table 7. Fitting results of parameters k and c to infiltration numbers.

Parameters	k	c	$Adj-R^2$
Expression	$k = 0.2664 \times n + 1.1984$	$c = -0.8519 \times n - 0.4779$	0.8028/0.7582

Then, under the repeated load after infiltration condition, the plastic strain mode was constructed using the parameters in Table 7, in which the infiltration numbers and loading repetitions were considered, as shown in Equation (5).

$$\varepsilon_p = (0.2664 \times n + 1.1984) \times N^{0.0521} + (-0.8519 \times n - 0.4779) \quad (5)$$

where ε_p is the plastic strain (10^{-3}), n is the infiltration number, and N is the number of loading repetitions.

Although the linear correlation coefficient was great at infiltration durations, the obtained results were not as good using the above method. This was mainly because the infiltration durations only had three analysis levels. The established calculation model would not reach great accuracy with three points. Considering the high similarities of the plastic strain variation under different conditions, Equation (2) was used as the initial model of plastic strain under different infiltration durations and loading repetitions. The fitting was carried out using Equation (2), and the values and differences in parameter b were small at various infiltration durations. Therefore, the average of parameter b was used as the representative value at different infiltration durations, which was taken at 0.0387. As for parameter a , a power function method was adopted. Then, taking the infiltration durations and repeated loads into account, a plastic strain calculation model was established, as shown in Equation (6).

$$\varepsilon_p = (2.7303 \times t^{0.0944}) \times N^{0.0387} \quad (6)$$

where ε_p is the plastic strain (10^{-3}), t is the infiltration duration (min), and N is the number of loading repetitions.

With Equations (5) and (6), the plastic strain was calculated at various infiltration conditions, as shown in Figure 10. There were obvious differences between the calculations and measurements of plastic strain under the repeated load after infiltration condition. The maximum difference was 0.9197×10^{-3} , accounting for 14.8% of the measurements at various infiltration numbers. When the infiltration duration was considered, the maximum difference was 2.016×10^{-3} , accounting for 64.28%. However, when the first 100 repetitions were removed, the maximum difference was 0.8847×10^{-3} , accounting for 18.7%. This showed that the calculation model considering infiltration numbers had greater accuracy than the model considering infiltration durations. The infiltration factors increased the complexity of the models. Compared with the repeated load only test, the error rate of the plastic strain models increased from 4.6% to 18.7% when infiltration was considered. On the other hand, the influence of infiltration numbers and durations was different on the plastic strain. Considering the infiltration durations, the calculation accuracy was lower, which was attributed to the limited level of duration. It was difficult to accurately describe the influence of infiltration duration with the insufficient dataset.

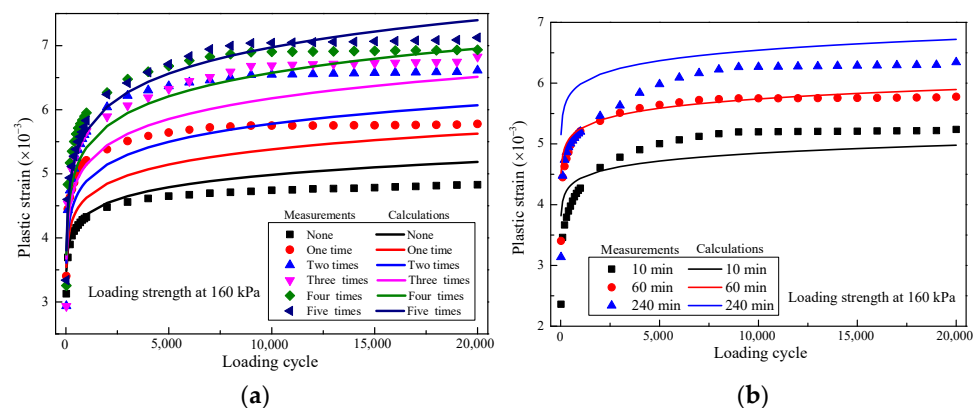


Figure 10. Plastic strain between measurements and calculations under different infiltration conditions: (a) infiltration numbers; (b) infiltration durations.

4.3. Simultaneous Action with Repeated Load and Infiltration

When repeated load and infiltration acted simultaneously, the plastic strain was obviously different from the previous two tests in Figure 2c. The plastic strain had the same level after two simultaneous actions. Then, the first and second simultaneous actions were the main considerations for the establishment of the calculation model. In the first and second simultaneous actions, the plastic strain appeared to exhibit a step-type change at the end and beginning of the next simultaneous action. According to the variation in plastic strain, a calculation model was constructed via the following steps.

Step 1: Establish the stage model of plastic strain under the first simultaneous action using the power model, as shown in Equation (2).

Step 2: Establish the second stage model using the Sigmoidal Logistic model for the residual plastic strain, which deducts the first calculated plastic strain from the whole plastic strain, as shown in Equation (7).

$$\sigma_0 \quad (7)$$

where a , k , and x_c are the model parameters, which can be obtained via regression.

Step 3: Establish the third stage model using the Sigmoidal Logistic model on the basis of the second stage if the third stage exists using the method in step 2.

Step 4: Establish the calculation model with linear superposition of the stage models under simultaneous action.

Taking the plastic strain under simultaneous action with 60 min infiltration as an example, the calculation model of plastic strain was constructed according to the above steps. First, a power function was used to establish the plastic strain model in the first stage, as shown in Equation (8). The number of loading repetitions ranged from 21 to 5,000 times.

$$\varepsilon_{p1} = 4.7747 \times N^{0.0197} \quad (Adj - R^2 = 0.8023) \quad (8)$$

Using Equation (8), the calculation was obtained in Figure 11a. Then, the plastic strain of the first stage was deducted from the total plastic strain. The residual plastic strain at the second stage was obtained as shown in Figure 11b, which can be fitted using the Sigmoidal Logistic model in Equation (7). The fitting correlation coefficient was up to 0.9797. This indicated that the Sigmoidal Logistic model can effectively describe the development of residual plastic strain in the second stage under the simultaneous action test. Through linear superposition of the models in the two stages, the calculation model can be obtained under simultaneous action test, as shown in Equation (9).

$$\varepsilon_p = 4.7747 \times N^{0.0197} + \frac{1.3556}{1 + e^{-0.0029 \times (N - 18761.48)}} \quad (9)$$

With Equation (8), the calculations and measurements under the simultaneous action test are shown in Figure 11c. In the second stage, the maximum difference between calculations and measurements was 0.6905×10^{-3} , accounting for 15.8% of the measurements. When the plastic strain in the first 100 repetitions was removed, the maximum difference during the 101 to 60,000 loading repetition was only 0.214×10^{-3} , accounting for 3.8% of the measurements. This indicated that the calculation model in Equation (9) had sufficient accuracy with the measurements under the simultaneous action test.

Using the above method, calculation models were established for infiltration with 10 min and 35 min, as shown in Equations (10) and (11).

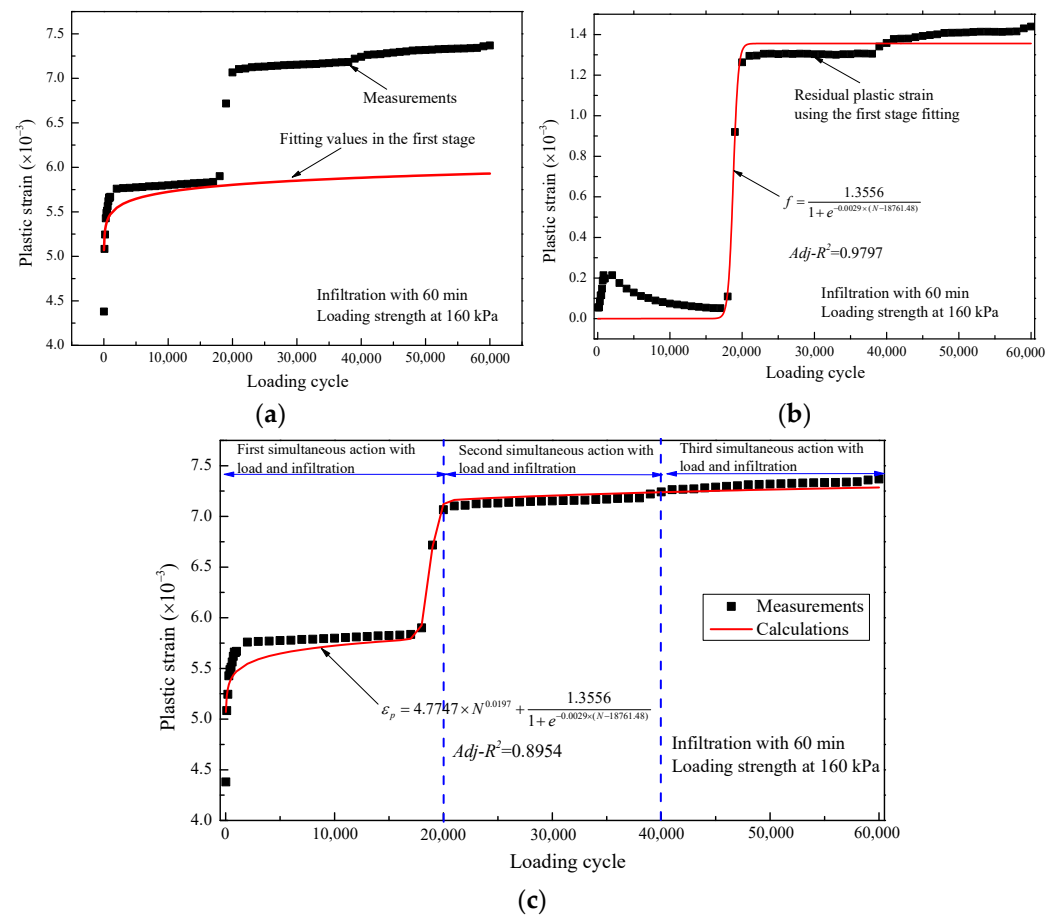


Figure 11. Plastic strain under simultaneous action with repeated load and 60 min infiltration: (a) fitting for the first stage; (b) the residual plastic strain for the second stage; (c) comparison between measurements and calculations.

When the infiltration duration was 10 min:

$$\epsilon_p = 3.3761 \times N^{0.0522} + \frac{0.9875}{1 + e^{-0.00085 \times (N - 21519.25)}} \quad (10)$$

When the infiltration duration was 35 min:

$$\epsilon_p = 3.7838 \times N^{0.0386} + \frac{1.5782}{1 + e^{-0.0017 \times (N - 11281.16)}} \quad (11)$$

Using Equations (10) and (11), the calculations and measurements at 10 min and 35 min infiltration were compared, as shown in Figure 12. This showed that the calculations for the two simultaneous actions were quite consistent with the measurements. With 10 min infiltration under the simultaneous action test, the differences were great during the first 100 loading repetitions; they were up to 1.8027×10^{-3} and accounted for 55.3%. However, the maximum difference was only 0.5714×10^{-3} and accounted for 11.5% when the loading repetitions ranged from 101 to 60,000. A similar situation occurred for the 35 min infiltration; the maximum difference was up to 1.2317×10^{-3} (accounting for 34.2%) during the first 100 loading repetitions, and it was only 0.5684×10^{-3} (accounting for 8.5%) among the subsequent loading repetitions. Via the comparative analyses, it can be concluded that the plastic strain under the simultaneous action test can be effectively calculated using Equations (9)–(11), which have reliable accuracy.

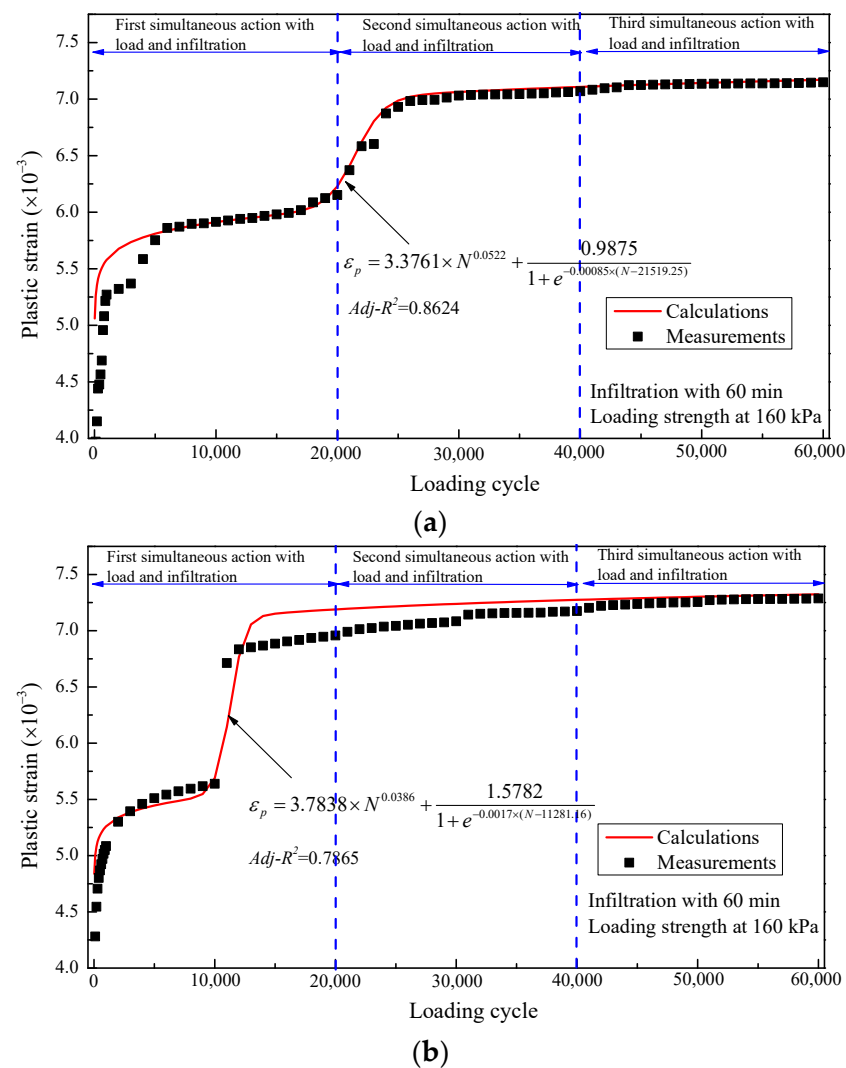


Figure 12. Plastic strain comparison between measurements and calculations under simultaneous action with repeated load and infiltration: (a) infiltration duration of 10 min; (b) infiltration duration of 35 min.

4.4. Discussions of Plastic Strain and Calculation Models

In this study, the plastic strain calculation models were consistent with the models in previous studies under the repeated load only test and repeated load after infiltration test. The power function model was found to work well with the variation in plastic strain. However, the power function model did not effectively characterize the variation in plastic strain under the simultaneous action test. It presented multistage variation, which was related to the multistage experimental plan. From this aspect, the simultaneous action had a significant influence on the plastic strain of the UGM. When the plastic strain was divided into three stages, each stage had the same variation as the repeat load only test and repeated load after infiltration test. This was related to the shakedown feature of the UGM. Therefore, it can be concluded that the power function model had a great advantage in describing plastic strain variation under various conditions.

As for the calculation model under the multistage repeated load, Erlingsson et al. established and reconstructed multistage models from some typical single-stage models, such as the models proposed by Korkiala-Tanttu, Gidel model Tseng and Lytton et al. [11,15,35,36]. Via their comparisons, Erlingsson et al. pointed out that the quality of fit was dependent on the specific model used [15]. It was accepted that different models had different efficiencies to predict plastic strain, which was also proven in this study. As for the different tests, the

calculation models had various expressions. Since the previous models included too many parameters, such as stress path, moisture content, elastic strain, total plastic strain, hydrostatic stress and deviator stress, the application of these models became a complicated choice for engineering. Compared with the model proposed by Erlingsson et al., the elements of the calculation model were simpler and more understandable in this study. Therefore, the proposed model is promising for plastic strain calculation in permeable pavement engineering.

On the other hand, the material composition is one decisive factor affecting the plastic strain of UGM, especially the structure type composed of coarse and fine aggregate. Although, in this study, the median gradation used in an unbound base was taken as an example to investigate the plastic strain under three working conditions, the variation tendency of plastic strain exhibits great similarities with various material compositions. In our previous works, a prediction model of plastic strain was proposed considering the material composition and loading conditions [17,18]. According to our verification and validation results, the proposed model had great accuracy. In addition, there were more than three working conditions that the UGM faced with repeated load and infiltration. The mentioned and selected working conditions had the advantages of operation and factor-controlling. As seen from the results, different working conditions may lead to various variations in the plastic strain of UGM, which could represent new points to find out the differences between them.

5. Conclusions

Considering the influence of repeated load and water infiltration on UGMs (unbound granular materials), three working conditions were assessed: repeated load only, repeated load after infiltration, and simultaneous action with load and infiltration. Tests were conducted using improved PUMA (precision unbound material analyzer) equipment. Plastic strain and plastic strain rate were taken as the indicators for deformation analyses. Calculation models of plastic strain were established under three working conditions. The main findings and conclusions were drawn as follows.

- (1) The plastic strain and plastic strain rate were proportional to the loading strength in the repeated load only test. The plastic strain increased and the plastic strain rate decreased with the increase in loading repetitions. Rapid changes occurred in the initial stage, but tended to stabilize after certain repetitions.
- (2) The variation trend of plastic strain and plastic strain rate under repeated load after infiltration was similar to that under the repeated load only test. The plastic strain had obvious increments with the increase in infiltration number, while the changes in plastic strain rate were relatively small. The first infiltration had a more significant effect on the plastic strain compared to the subsequent infiltrations. Longer infiltration durations led to the greater plastic strain, but had a smaller impact on the plastic strain rate. When the infiltration duration exceeded 240 min, further verification and analyses became necessary.
- (3) When infiltration and repeated load acted simultaneously, the plastic strain exhibited distinct variation compared to the previous two tests. The plastic strain increased towards the end of the infiltration process. Significant changes in plastic strain occurred during the first and second simultaneous actions, while it tended to stabilize during the third simultaneous action. The plastic strain rate under the simultaneous action test followed a similar pattern to that observed in the previous two tests.
- (4) A power function model served as a base model to establish the calculation model of plastic strain in the three tests. Considering the loading strength and repetitions, a calculation model was established at the repeated load only test with an error of 4.6%. Taking the infiltration numbers and durations into account, two separate calculation models were developed, which presented varying accuracies with errors at 18.5% and 8.5%, respectively.
- (5) Power function and Sigmoidal Logistic models were used to construct the calculation models under simultaneous action. The proposed calculation models had great accu-

racy, with the maximum error being only 11.5%, ranging from 100 to 60,000 repetitions. Overall, the calculations showed an acceptable level of accuracy within 15% compared with the measurements. These calculation models can very effectively characterize plastic strain under the three working conditions, and consider the loading strength, loading repetitions, infiltration numbers and durations.

Author Contributions: Conceptualization, N.L., D.H. and J.W.; methodology, N.L. and X.Z.; formal analysis, N.L., X.Z. and D.H.; investigation, N.L. and X.Z.; resources, X.Z. and J.W.; data curation, X.Z.; writing—original draft preparation, N.L. and X.Z.; writing—review and editing, X.Z. and D.H. All authors have read and agreed to the published version of the manuscript.

Funding: The support from Opening Funding by the Key Laboratory of Transport Industry of Road Structure and Material (Research Institute of Highway, Ministry of Transport) (No. 0220KY99ZY052-01), the Natural Science Basic Research Program of Shaanxi (No. 2022JQ-560 and No. 2022JQ-394) and the National Natural Science Foundation of China (No. 52308465) is greatly appreciated.

Institutional Review Board Statement: Not applicable.

Informed Consent Statement: Not applicable.

Data Availability Statement: The data presented in this study are available on request from the corresponding author. The data are not publicly available because they are part of an ongoing study.

Conflicts of Interest: The authors declare no conflict of interest.

References

1. Qin, Y. A review on the development of cool pavements to mitigate urban heat island effect. *Renew. Sustain. Energy Rev.* **2015**, *52*, 445–459. [\[CrossRef\]](#)
2. Guan, X.; Wang, J.; Xiao, F. Sponge city strategy and application of pavement materials in sponge city. *J. Clean. Prod.* **2021**, *303*, 127022. [\[CrossRef\]](#)
3. Santamouris, M. Using cool pavements as a mitigation strategy to fight urban heat island—A review of the actual developments. *Renew. Sustain. Energy Rev.* **2013**, *26*, 224–240. [\[CrossRef\]](#)
4. Li, H.; Li, Z.; Zhang, X.; Li, Z.; Liu, D.; Li, T.; Zhang, Z. The effect of different surface materials on runoff quality in permeable pavement systems. *Environ. Sci. Pollut. Res.* **2017**, *24*, 21103–21110. [\[CrossRef\]](#) [\[PubMed\]](#)
5. Lu, G.; Wang, H.; Törzs, T.; Liu, P.; Zhang, Y.; Wang, D.; Oeser, M.; Grabe, J. In-situ and numerical investigation on the dynamic response of unbounded granular material in permeable pavement. *Transp. Geotech.* **2020**, *25*, 100396. [\[CrossRef\]](#)
6. Ma, G.; Li, H.; Yang, B.; Zhang, H.; Li, W. Investigation on the deformation behavior of open-graded unbound granular materials for permeable pavement. *Constr. Build. Mater.* **2020**, *260*, 11980. [\[CrossRef\]](#)
7. Brunetti, G.; Šimůnek, J.; Piro, P. A comprehensive numerical analysis of the hydraulic behavior of a permeable pavement. *J. Hydrol.* **2016**, *540*, 1146–1161. [\[CrossRef\]](#)
8. Ishikawa, T.; Zhang, Y.; Tokoro, T.; Miura, S. Medium-size triaxial apparatus for unsaturated granular subbase course materials. *Soils Found.* **2014**, *54*, 67–80. [\[CrossRef\]](#)
9. Sangsefidi, E.; Larkin, T.J.; Wilson, D.J. The effect of weathering on the engineering properties of laboratory compacted unbound granular materials (UGMs). *Constr. Build. Mater.* **2021**, *276*, 122242. [\[CrossRef\]](#)
10. Nazzal, M.D.; Mohammad, L.N.; Austin, A.; Al Hosainat, A. Effect of moisture content on the shakedown limits of base course materials. *Transp. Res. Rec.* **2021**, *2675*, 192–202. [\[CrossRef\]](#)
11. Tseng, K.H.; Lytton, R.L. *Prediction of Permanent Deformation in Flexible Pavements Materials, Implication of Aggregates in the Design, Construction, and Performance of Flexible Pavements* ASTM STP 1016; American Society for Testing and Materials (ASTM): West Conshohocken, PA, USA, 1989; pp. 154–172.
12. Lekarp, F.; Dawson, A. Modelling permanent deformation behaviour of unbound granular materials. *Constr. Build. Mater.* **1998**, *2*, 9–18. [\[CrossRef\]](#)
13. Werkmeister, S.; Dawson, A.R.; Wellner, F. Permanent deformation behaviour of granular materials. *Road Mater. Pavement.* **2005**, *6*, 31–51. [\[CrossRef\]](#)
14. Hornych, P.; Chazallon, C.; Allou, F.; El Abd, A. Prediction of Permanent Deformations of Unbound Granular Materials in Low Traffic Pavements. *Road Mater. Pavement.* **2007**, *8*, 643–666. [\[CrossRef\]](#)
15. Erlingsson, S.; Rahman, M.S. Evaluation of permanent deformation characteristics of unbound granular materials by means of multistage repeated-load triaxial tests. *Transp. Res. Rec.* **2013**, *2369*, 11–19. [\[CrossRef\]](#)
16. Araya, A.; Huurman, M.; Molenaar, A. Integrating traditional characterization techniques in mechanistic pavement design approaches. In Proceedings of the Transportation and Development Institute Congress 2011: Integrated Transportation and Development for a Better Tomorrow, Chicago, IL, USA, 13–16 March 2011; pp. 596–606.

17. Li, N.; Ma, B.; Wang, J. Quantitative characterization of significant nonlinear stage of elasto-plastic deformation of unbound granular materials under repeated loads. *J. Highway Transport. Res. Develop.* **2023**, *40*, 68–77+87.
18. Li, N.; Wang, X.; Qiao, R.; Ma, B.; Shao, Z.S.; Sun, W.; Wang, H. A prediction model of permanent strain of unbound gravel materials based on performance of single-size gravels under repeated loads. *Constr. Build. Mater.* **2020**, *246*, 118492. [[CrossRef](#)]
19. Zhang, D.; Huang, X.; Zhao, Y. Investigation of the shape, size, angularity and surface texture properties of coarse aggregates. *Constr. Build. Mater.* **2012**, *34*, 330–336. [[CrossRef](#)]
20. Gu, F.; Zhang, Y.; Luo, X.; Sahin, H.; Lytton, R.L. Characterization and prediction of permanent deformation properties of unbound granular materials for Pavement ME Design. *Constr. Build. Mater.* **2017**, *155*, 584–592. [[CrossRef](#)]
21. Ma, B.; Mo, S.; Wang, B. Rational range determination of key sieve pores for graded crushed stone based on shear performance. *J. Traffic Transp. Eng.* **2005**, *5*, 27–31.
22. Li, W.; Zheng, N.; Fu, H. Study of drainage performance of graded crushed stone and base drainage system. *J. Highway Transp. Res. Develop.* **2010**, *27*, 11–16.
23. Kazemi, F.; Hill, K. Effect of permeable pavement basecourse aggregates on stormwater quality for irrigation reuse. *Ecol. Eng.* **2015**, *77*, 189–195. [[CrossRef](#)]
24. Xiao, Y.; Chen, L.; Zhang, Z.; Lyu, D.; Tutumluer, E.; Zhang, J. Laboratory validation of a gradation design concept for sustainable applications of unbound granular materials in pavement construction. *Constr. Build. Mater.* **2016**, *129*, 125–139. [[CrossRef](#)]
25. Xiao, Y.; Tutumluer, E.; Mishra, D. Performance evaluations of unbound aggregate permanent deformation models for various aggregate physical properties. *Transp. Res. Rec.* **2015**, *2525*, 20–30. [[CrossRef](#)]
26. Li, N.; Tian, Y.; Ma, B.; Hu, D. Experimental investigation of water-retaining and mechanical behaviors of unbound granular materials under infiltration. *Sustainability* **2022**, *14*, 1174. [[CrossRef](#)]
27. *JTG E42-2005*; The Methods of Aggregate for Highway Engineering. China Communications Press: Beijing, China, 2005.
28. *JTG F20-2015*; Technical Guidelines for Construction of Highway Roadbases. China Communications Press: Beijing, China, 2015.
29. *JTG E40-2007*; Test Methods of Soil for Highway Engineering. China Communications Press: Beijing, China, 2007.
30. D'Angelo, G.; Thom, N.H.; Presti, D.L. Bitumen stabilized ballast: A potential solution for railway track-bed. *Constr. Build. Mater.* **2016**, *124*, 118–126. [[CrossRef](#)]
31. Kwon, J.; Kim, S.H.; Tutumluer, E.; Wayne, M.H. Characterization of unbound aggregate materials considering physical and morphological properties. *Int. J. Pavement Eng.* **2017**, *18*, 303–308. [[CrossRef](#)]
32. Liu, Y. Research on Performance of Unbound Granular Flexible Base. Master's Thesis, Chongqing Jiaotong University, Chongqing, China, 2008.
33. Chen, G.B. Study on the Permanent Deformation Prediction Model of Graded Crushed Stone through Simulations. Master's Thesis, Chang'an University, Xi'an, China, 2009.
34. Xiao, Y.; Zheng, K.; Chen, L.; Mao, J. Shakedown analysis of cyclic plastic deformation characteristics of unbound granular materials under moving wheel loads. *Constr. Build. Mater.* **2018**, *167*, 457–472. [[CrossRef](#)]
35. Gidel, G.; Horny, P.; Chauvin, J.J.; Breyse, D.; Denis, A. A New Approach for Investigating the Permanent Deformation Behaviour of Unbound Granular Material Using the Repeated Load Triaxial Apparatus. *Bull. Liaison Lab. Ponts Chaussées* **2001**, *233*, 5–21.
36. Korkiala-Tanttu, L. A New Material Model for Permanent Deformations in Pavements. In Proceedings of the 7th Conference on Bearing Capacity of Roads, Railways, and Airfields, Trondheim, Norway, 25–27 June 2005.

Disclaimer/Publisher's Note: The statements, opinions and data contained in all publications are solely those of the individual author(s) and contributor(s) and not of MDPI and/or the editor(s). MDPI and/or the editor(s) disclaim responsibility for any injury to people or property resulting from any ideas, methods, instructions or products referred to in the content.